Lateral resistance of polyurethane-reinforced ballast with the application of new bonding schemes

Laboratory tests and discrete element simulations

Jing, Guoqing; Zhang, Xu; Jia, Wenli

DOI
10.1016/j.conbuildmat.2019.06.114

Publication date
2019

Document Version
Accepted author manuscript

Published in
Construction and Building Materials

Lateral resistance of polyurethane-reinforced ballast with the application of new bonding schemes: laboratory tests and discrete element simulations

Guoqing Jing[a], Xu Zhang[b,]* & Wenli Jia[c]

[a] School of Civil Engineering, Beijing Jiaotong University, Beijing 100044, China

[b] School of Civil and Transportation Engineering, Guangdong University of Technology, Guangzhou 510006, China

[c] Faculty of Civil Engineering and Geosciences, Delft University of Technology, Delft, 2628CN, Netherlands

* Corresponding author, e-mail: xuzhang@gdut.edu.cn

Abstract: To mitigate the ballast flight risk in the high-speed railway, this paper presents three new polyurethane bonding schemes which have negligible influence to tamping operations. With the application of these bonding schemes, a series of laboratory tests indicated that the polyurethane-reinforced ballast exhibited much larger lateral resistance than the ordinary ballast by 31% at least. Discrete element simulation results further demonstrated that the polyurethane improved the load-bearing capacity of the ballast at the particle scale through effectively restraining the particle movement. Therefore, the proposed bonding schemes ensure adequate lateral ballast resistance and are effective measures for improving the ballast performance.

Key words: high-speed railway; ballast; polyurethane; discrete element method; lateral resistance; single sleeper pull-out test

1. Introduction

Railway ballast is often constructed using crushed stones and works as an important granular layer under the track superstructure. One of the main functions of the ballast layer is to provide sufficient lateral resistance to the track panel so that the track geometry and stability can be kept and the train running safety can be ensured. Insufficient lateral ballast resistance may lead to some serious problems such as excessive movement of the track panel and track lateral buckling [1]. In order to provide enough lateral ballast resistance to the track, numerous measures have been taken all over the world to reinforce the ballast especially since the extensive application of the continuously welded rail (CWR) track which requires large lateral ballast resistance to prevent the track from bulking [2-6]. Among these measures, increasing the height of the shoulder ballast to be 100-150 mm over the ballast surface is considered as an effective way in China and many other countries for years.

However, with the rapid development of the high-speed railways over the past few years, the high shoulder ballast brings a new problem. It was reported that the shoulder ballast stones may fly due to the strong wind caused by the high-speed trains, and this phenomenon becomes a severe problem in the railways whose design speed reaches or exceeds 350 km/h [7,8]. Except for the shoulder ballast, the surface ballast stones near the sleeper centre also may fly easily due to the strong negative air pressure formed under the high-speed train bogies [7,9]. The ballast stones blowing up from the track during the train passage would probably strike the train components and the rail heavily which further results in failure or damage problems to the train and the rail [10]. From the perspective of mitigating the ballast flight due to the high speed running of the trains, the height of the shoulder ballast should be decreased just as the flat ballast shoulder adopted in European railways. But regarding that the shoulder and crib ballast play important roles in the lateral ballast resistance [11], decreasing the height of the shoulder ballast will reduce the lateral ballast resistance to some extent though it is indeed helpful in mitigating the ballast flight. When the shoulder ballast height is decreased, other measures should be taken to gain enough lateral ballast resistance.

Aiming at this issue, the polyurethane, a kind of polymer material, has been applied to reinforce the ballast in recent years by bonding the granular ballast particles as a massive structure. To investigate the mechanical properties and performance of the polyurethane-reinforced ballast, a few laboratory and field tests have been conducted by researchers. According to the triaxial test results, Lee et al. [12] figured out that both the shear strength and the elastic moduli of the polyurethane-mixed ballast increase linearly with the content of the polyurethane. Woodward et al. [13-15] and Kennedy et al. [16] reported laboratory tests and engineering practices to show the applications of the polyurethane to help maintain track geometry and absolute clearances, to improve the ballast stiffness and to reduce the ballast settlement. Woodward et al. [17] and Kruglikov et al. [18] presented that the lateral resistance of the ballast increased remarkably after the shoulder ballast was reinforced with the polyurethane along the longitudinal direction to form a block wall at the track side. Thomas et al. [19] demonstrated an application of the polyurethane to obtain more uniform load distribution of the ballasted track on a masonry bridge. These studies demonstrate that the polyurethane has been successfully applied to reinforce the railway ballast for many different goals. The relevant test results and engineering practices indicate that the application of the polyurethane really improves the ballast performance effectively.

Focusing on mitigating the ballast flight risk in high-speed railways, the polyurethane is often sprayed across the whole ballast surface. Fig. 1 illustrates the sketch of the widely adopted bonding scheme. Since all the particles from the surface to a certain depth in the ballast layer are strongly bonded by the polyurethane, this bonding scheme is effective in avoiding the ballast flight even in the cases when the trains run at very high speeds. However, this bonding scheme has an obvious disadvantage of affecting the tamping operations significantly. Because when all the surface ballast particles are entirely bonded with the polyurethane, it is quite difficult to insert the arms of the tamping machines into the bonded ballast to a required depth. New bonding schemes that can avoid the ballast flight and have negligible influence to the tamping operations simultaneously are very desirable for reinforcing the ballast in the high-speed railways. Meanwhile, although lots of studies have proved that it is effective to reinforce the ballast with the polyurethane, the mechanisms that how the polyurethane affects the micro-mechanical behaviours of the ballast have not been revealed yet, which still needs further insightful research.

2 New bonding schemes for reinforcing the ballast with polyurethane

This paper proposes three new bonding schemes, denoted as E, C & B, respectively, for reinforcing the high-speed railway ballast with the polyurethane. In these new bonding schemes, only the ballast in four target regions instead of all the surface ballast are required to be bonded with the polyurethane. Fig. 2 demonstrates the four target regions where the ballast shall be bonded. Among these regions, two are at the sleeper ends and the other two are near the sleeper centre. In the proposed bonding scheme E, the shoulder ballast near the two sleeper ends are required to be bonded. In the bonding scheme C, the crib ballast near the sleeper centre shall be bonded, and in the bonding scheme B, both the ballast in the sleeper end and centre areas are required to be bonded.

Since the target regions in Fig. 2 almost cover all the dangerous areas where the ballast flight is likely to occur, the new bonding schemes meet the requirement of avoiding the ballast flight by bonding the particles in these dangerous regions with the polyurethane. In the meantime, the new bonding schemes do not require the application of the polyurethane to the ballast in the areas near the rails where the tamping machines always work. Hence, the new bonding schemes have negligible influence to the tamping operations to the ballast. It is also worthy being noted that as indicated by the dimensions in Fig. 2, the target bonding regions in the three new bonding schemes are just 18.1%, 7.2%, and 25.3%, respectively, of the whole ballast surface, which can help reduce the dosage of the polyurethane distinctly. Also, with the new bonding schemes, the height of the ballast shoulder can be decreased, which reduces the dosage of the ballast material. Therefore, relative to the conventional bonding scheme, the new bonding schemes are more economical in the dosage of the ballast and the polyurethane material. In a word, the proposed bonding schemes simultaneously have multiple advantages of avoiding the ballast flight, reducing the dosage of the polyurethane and having negligible influence to the tamping operation.

However, the new bonding schemes have much smaller bonding area than the conventional scheme, and the ballast shoulder height is cancelled, both of which bring about a problem that whether the lateral resistance of the ballast locally reinforced with the polyurethane based on the new bonding schemes is enough to keep the track lateral stability or not? Aiming at this issue, laboratory tests and discrete element simulations were carried out in this paper to investigate the lateral resistance of the ballast locally reinforced with the polyurethane based on the proposed bonding schemes. Two different bonding depth of 200 mm and 300 mm in the ballast were studied in the tests to investigate the feasibility of the new bonding schemes in providing enough lateral resistance for the high-speed railway track. Furthermore, the discrete element method (DEM) was employed in this paper to study the micro-mechanical behaviours of the ballast reinforced with the polyurethane since the DEM has the advantage in simulating the mechanical behaviours of granular materials. The mechanism that how the polyurethane materials helps increase the lateral ballast resistance was also studied and revealed through the DEM analyses.

3 Laboratory tests on the lateral resistance of polyurethane-reinforced ballast

The single sleeper pull-out test (SSPT) is an effective and frequently used method to evaluate the ballast resistance. In order to evaluate the lateral resistance of the ballast locally reinforced with the polyurethane, a series of laboratory tests were carried out using a full-scale test track and will be presented in this section.

3.1 Material properties of ballast and polyurethane

The ballast material adopted in the test is basalt with the particle size gradation illustrated in Fig. 3, which meets the requirement of the ballast gradation standard in China. The polyurethane material utilized in this test was jointly developed by Beijing Jiaotong University and State Key Laboratory of Special Functional Waterproof Materials (SKLSFWM) in China. The polyurethane was produced by mixing two components, namely the component A-isocyanate & the component

B-polyols, with the volume ratio of 1:1. The strength of the produced polyurethane rapidly reaches 70% of its final strength one day after the mixing and continues to increase with the time. The mechanical parameters of the polyurethane were measured in SKLSFWM and listed in Table 1.

3.2 Test facility

A full-scale test track comprising of sleepers and ballast was established in Beijing Jiaotong University. The total length of the test track was 12 m. The thickness of the ballast under the sleeper was 350 mm and the total width of the ballast bed was 3,600 mm. The width of the ballast shoulder was 500 mm and the slope was 1:1.75. The dimensions of the test track were consistent with those in the high-speed railway ballasted track in China.

The construction procedures of the test track are described hereinafter. Firstly, the ballast material were compacted in four layers with an electronic plate compactor to form the dense ballast bed. Then, the type IIIc pre-stressed concrete sleepers, which are frequently adopted for the ballasted track in China's high-speed railways, were laid on top of the ballast with the spacing of 600 mm. After that, extra ballast material was put between the adjacent sleepers and at the sleeper ends, and compacted in three layers to form the crib and shoulder ballast. Finally, the polyurethane was sprayed from the top surface of the ballast using a specialized spray gun. The polyurethane then went down into the ballast to form coating on the surface of the ballast particles and bond the particles at the contacts.

Fig. 4 shows the photographs of the test track with and without the reinforcement of the polyurethane. For each of the three proposed bonding schemes, two test tracks with different bonding depth in the ballast, i.e. 200 mm and 300 mm, were constructed by controlling the dosage of the polyurethane material. As a reference, two extra test tracks were constructed without the reinforcement of the polyurethane. The summary of the laboratory tests that were carried out is listed in Table 2. Among all the eight tests, the shoulder ballast height was only set in the test ‘Ns’, which represents the typical ballasted track in China with the shoulder ballast height of 150 mm. By comparing the results in the tests ‘Ns’ and ‘Nf’ that were carried out on the unreinforced ballast, the effect of the shoulder ballast height on the lateral resistance can be studied. For the other six tests, the first capital letters in their test names indicate the bonding scheme as discussed in Section 2 and the numbers after the capital letters indicate the bonding depth is 200 or 300 mm.

3.3 Test apparatus and procedures

A set of specialized apparatus consisting of an oil pump, a force transducer, a reaction frame, two dial indicators and a data logger was developed and adopted to measure the lateral resistance force of the ballast and the lateral displacement of the sleeper in the SSPT. Fig. 5 presents the apparatus utilized for the measurement in the test.

In order to pull out the sleeper, the oil pump together with the force transducer and the reaction frame was horizontally installed at one sleeper end. The dial indicators were fixed above the sleeper with their pointers parallel to the sleeper. In the test, the oil pump was controlled to apply multi-stage loads to the sleeper. When the sleeper moved slowly under the horizontal load, the lateral force measured by the force transducer and the lateral displacement measured by the dial indicators were collected and saved in the data logger. Each load stage continued until the sleeper displacement increased to a stable value, and then the next stage of load was applied. Each test did not stop until the state that the lateral resistance force of the ballast almost kept stable. After each sleeper pull-out test, the test track including the ballast was dismantled and re-established with the same method as described in Section 3.2 for the next test, which ensured close ballast densities in all tests. Moreover, three repetitive tests were carried out for each test condition in Table 2. The measured results of the three tests were averaged as the test result for that load condition, and will be presented in the paper.

3.4 Test results

Fig. 6 illustrates the lateral resistance force *F* of the reinforced ballast as a function of the lateral sleeper displacement *d* for the three new bonding schemes. In each subplot, the results of the tests 'Ns' and 'Nf' are also presented for comparison. It can be found the resistance force increases rapidly with the lateral sleeper displacement at the initial stage, and then gradually becomes stable when the sleeper displacement continues to increase. The lateral resistance force in the test 'Ns' is distinctly larger than that in the test 'Nf', which demonstrates the important contribution of the 150 mm shoulder height to the lateral ballast resistance.

It also can be seen that the lateral resistance forces of the reinforced ballast based on all the three bonding schemes are remarkably larger than those in the tests 'Ns' and 'Nf'. For the same bonding scheme, the larger lateral resistance force was gained for the reinforced ballast with the deeper bonding depth of 300 mm. These results indicate the application of polyurethane does result in distinct increase to the lateral ballast resistance. Furthermore, the deeper the ballast is bonded with the polyurethane, the larger is the lateral resistance of the reinforced ballast, which can be even larger than that of the unreinforced ballast with the shoulder height of 150 mm.

The lateral resistance force at the sleeper displacement of 2 mm obtained in the single sleeper pull-out test is always used for the quantitative evaluation of the lateral ballast resistance in practical engineering. To further quantify the lateral ballast resistance in the tests, the resistance forces at *d*=2 mm were collected from the measured results in Fig. 6 and listed in Table 3. The relative differences between the lateral resistance forces of the reinforced ballast and those in the tests 'Ns' and 'Nf' were also calculated and listed in the table. It can be found when the sleeper displacement reached 2 mm, the resistance forces of the ballast were 10.02 kN and 7.05 kN, respectively, in the tests ‘Ns’ and ‘Nf’. Apparently, without the ballast shoulder height, the lateral resistance force of the ballast decreases by nearly 30%.

When the ballast particles near the sleeper ends were bonded with the polyurethane, the lateral resistance force of the reinforced ballast with the bonding depth of 200 mm in the test ‘E2’ increased by 41% relative to the test ‘Ns’ and by 60% relative to the test ‘Nf’. With the deeper bonding depth of 300 mm in the test ‘E3’, the lateral resistance force increased by 100% relative to the test ‘Ns’, and by 128% relative to the test ‘Nf’.

When the ballast near the sleeper centre was reinforced with the polyurethane with the bonding depth of 200 mm, the increase of the ballast lateral resistance force in the test ‘C2’ was 41% in contrast to that in the test ‘Ns’ and was 60% comparing with that in the test ‘Nf’. With the deeper bonding depth of 300 mm in the test ‘C3’, the lateral resistance force increased by 41% relative to that in the test ‘Ns’, and by 100% relative to that the test ‘Nf’.

When both the ballast near the sleeper ends and the sleeper centre were simultaneously reinforced with the bonding depth of 200 mm, the lateral resistance force in the test ‘B2’ increased by 70% with respect to the test ‘Ns’ and by 142% with respect to the test ‘Nf’. When the bonding depth was 300 mm, the ballast resistance in the test ‘B3’ increased by 100% with respect to the test ‘Ns’ and by 184% with respect to the test ‘Nf’.

Obviously, the lateral resistance force increased by 31% at least in the tests when the ballast was reinforced with the polyurethane with the application of the three new bonding schemes. The lateral resistance force of the reinforced ballast in the test ‘C2’ with the bonding depth of 200 mm was the minimum, which was 13.09 kN. But it was still larger than the specified minimum value of 12 kN for the ballast in China’s high-speed railways with the design speed higher than 250 km/h [20]. It means the lateral ballast resistances based on all the three new bonding schemes are adequate to prevent the track from buckling.

Among the three bonding schemes, the maximum increment of the lateral resistance force was observed when the ballast was reinforced at both areas near the sleeper ends and its centre due to the largest bonding area in that case. In addition, comparing with the tests in which the bonding depth was 200 mm, the lateral resistance force of the reinforced ballast with the bonding depth of 300 mm was larger by 14% when the ballast near the sleeper ends was reinforced, by 8% when the ballast near the sleeper centre was reinforced and by 17% when the ballast at both areas was reinforced. It can be concluded that the larger area and the larger thickness of ballast is reinforced with the polyurethane, the larger lateral ballast resistance can be gained.

4 Discrete element simulations on the lateral resistance of polyurethane-reinforced ballast

The DEM is a numerical method that excels in simulating the mechanical behaviours of the granular material. It was firstly developed by Cundall and Strack [21] and has been successfully applied to simulate the mechanical behaviours of railway ballast [22-27]. With the DEM, the contact forces between granular particles and the particle movement can be simulated, which is really helpful to investigate the micro-mechanical behaviours of the granular material.

The laboratory tests have shown distinct increase of the ballast resistance force when the ballast is reinforced with the polyurethane. In order to reveal the micro mechanism that how the polyurethane helps improve the lateral ballast resistance, the commercial DEM software Particle Flow Code (PFC) was employed in this paper to simulate the SSPTs. The PFC deals with the contact forces between particles based on the classic contact laws, and it calculates particle movement according to Newton’s Second Law [28]. It also provides bond models to simulate the bonding behaviour between discrete particles, which can be used to simulate the bonding effect of the polyurethane to the ballast particles. The DEM models that simulate the laboratory test track including the polyurethane-reinforced ballast and the simulation results on the SSPTs will be presented and discussed in this section.

4.1 Discrete element modelling of ballast particles and polyurethane

The ballast particles always have irregular shapes and angular corners since they are stones mechanically crushed from intact rock. With the irregular shapes, the ballast particles interlock with each other to keep the ballast stability after they are compacted in the track. To simulate the contact and interlock behaviour between ballast particles well, discrete elements that can capture the realistic ballast particle shapes are desirable for the DEM modelling. In this research, rigid clumps with realistic particle shapes were generated with the laser scanning technique and the multi-sphere overlapping algorithm to simulate the ballast particles. Similar methods can be found in Refs. [26,29].

The procedures for generating the clumps are described here. First of all, three-dimensional images of real ballast particles were obtained using a handheld laser scanner-FreeScan X3, as shown in Fig. 7. Then, the images were imported into PFC to illustrate the particle surface, and the volume enclosed by each particle surface was completely filled with several overlapping spheres. Lastly, the irregular particle shape was approximated using a sufficient number of spheres with different diameters, and these overlapping spheres were regarded as a clump in the DEM simulation. In the present study, 20 real ballast particles with different shapes and size were scanned. Fig. 8 presents the different particle shapes and the corresponding clumps generated in PFC. The number of the spheres composing each clump are also presented in the figure. Since there are a large number of ballast particles in the test track, these clumps were repeatedly used for the DEM modelling.

Utilizing the clumps, the contact behaviours between ballast particles were simulated with the linear contact model which allowed sliding between the contacting clumps. Besides, in order to simulate the ballast reinforced with the polyurethane, the bonding effects that the polyurethane provided to the ballast particles were modelled by creating parallel bonds at the particle contact points. When loading, these bonds can generate bond forces and moments to restrict the relative movements of the contacting particles. The bond forces and moments were linearly determined by the bond stiffness, the bond area and the particle relative movements according to the linear parallel bond (LPB) model which was implemented in PFC. The details of the LPB model can be found in the PFC manual [28]. Furthermore, the polyurethane material has a finite strength after enough curing time and it may fracture when the reinforced ballast subjects to large external load. The fracture behaviour of the polyurethane was also modelled with the LPB model. It means the parallel bond breaks when the normal or shear stress on the bond induced by the bond forces and moments exceeds the specified strength.

4.2 Discrete element simulations of SSPTs on ballast reinforced with polyurethane

To simulate the SSPTs conducted in the laboratory, a 3D DEM model, as illustrated in Fig. 9a, was firstly established to simulate the sleeper and the ballast in the test track without any reinforcement. For the type IIIc sleeper, a stereo lithography (STL) file of the sleeper geometry was generated in the software AutoCAD and imported into PFC. Then wall elements were generated to reproduce the sleeper geometry. For the ballast, 45,355 clumps were generated according to the particle size distribution of the ballast in laboratory tests and compacted to achieve a desirable density. The side and base boundaries of the model were simulated using rigid wall elements. The dimensions of the DEM model were consistent with the test track except that only one sleeper bay was modelled here to reduce the simulation time while the laboratory test track has a total length of

12 m. In addition, after the DEM model was established, the sleeper was controlled to move down according to the numerical servo mechanism in PFC^{3D} until the total vertical reaction force applied to the sleeper base reached 2.7 kN which was equivalent to the weight of a real sleeper.

Based on this DEM model, parallel bonds were created to further simulate the ballast reinforced with the polyurethane. Since not all the ballast particles were bonded with the polyurethane in the laboratory tests, the parallel bonds were only created at the contacts between the ballast particles that were located in the specified bonding region and depth according to each bonding scheme. Thus, the DEM models in which the ballast particles in specified areas were bonded with the parallel bonds were established to simulate the test tracks reinforced with the polyurethane to the depth of 200 mm, as illustrated in Fig. 9.

The main parameters in the DEM models were listed in Table 4. The contact stiffness of the particle-sleeper contacts were set much larger than that of the particle-particle contacts. It should be pointed out that in the laboratory tests, the polyurethane material was manually sprayed from the ballast top surface and automatically went down to the ballast voids due to its fluidity. Based on this fact, it can be inferred that the bond effects of the polyurethane were uniform in the whole ballast layer. Given the inhomogeneity of the bonding effects in the test track, the parallel bond stiffness and strength in the DEM model were assumed to follow the Gaussian distribution. The mean value of the normal bond strength was determined according the tensile strength of the polyurethane listed in Table 1. For various bonding schemes, the same values of the micro-mechanical parameters were used in the DEM models while the parallel bonds were created in different regions.

After the DEM models were established and cycled to equilibrium states, the simulations of the SSPTs were performed by moving the sleeper along the lateral track direction at a speed of 4 mm/s. This speed was set to be larger than that in the laboratory tests to save the computational time, and the damping coefficient in the model was set to 0.5 to eliminate the dynamic effect due to the large moving speed. The maximum lateral displacement was set to 3 mm because the laboratory test results showed that the lateral resistance forces of the reinforced ballast were almost stable when the lateral displacement exceeded 3 mm. During the simulations, the lateral displacement of the sleeper and the lateral resistance force which was the lateral component of the sum of the contact forces between the sleeper and ballast particles were monitored to investigate the lateral ballast resistance responses.

4.3 Validation of discrete element models

Fig. 10 presents the simulation results of the lateral resistance force-displacement responses of the reinforced ballast under various bonding schemes using the DEM models. The laboratory test results were also presented in the figure for comparison. It can be seen that the DEM results have good agreement with the test results when the sleeper displacement exceeds 2 mm, but there are obvious differences between them in the initial phase. A possible reason for the difference is that the large sleeper moving speed in the DEM simulations may resulted into reasonable dynamic effect to the ballast which was not fully eliminated even though the global damping coefficient of 0.5 had been considered. Meanwhile, the bonding behaviour of the polyurethane is quite complicated and may have large variations under different conditions. Lacking of the knowledge on the micro mechanical behaviours of the polyurethane bonds, a simple LPB model was adopted in the DEM simulations. To better capture the responses in the initial phase, the particle contact behaviours and the local bonding effects that the polyurethane applied to the ballast should be further investigated in the future.

Overall, the DEM results exhibit similar increase trends and close stable values with the test results for all the four bonding cases. When the lateral sleeper displacement reaches 2 mm, the ballast resistance forces in the DEM results are 7.27, 14.30, 13.24 and 17.16 kN, respectively, for the unreinforced ballast and that reinforced at the sleeper ends, centre and both areas. These values are quite close to those measured in the tests as listed in Table 3. Hence, the established DEM models for the unreinforced and reinforced ballast are reasonable and can reproduce the lateral resistance force-displacement responses with good accuracy.

4.4 Micro-mechanical behaviour analysis

In order to reveal the mechanism that how the polyurethane improves the ballast resistance, the micro-mechanical behaviours of the ballast in the SSPTs are discussed hereinafter. According to the DEM simulation results, the maximum particle displacement and distributions of the contact force chains in the reinforced ballast are compared with those in the ordinary ballast without reinforcement to show the restraints that the polyurethane provides to the ballast at the particle scale.

Fig. 11 illustrates the force chain distributions in the ballast from different view angles when the lateral sleeper displacement reaches 3 mm. In this figure, solid lines are plotted at the particle contact points to represent the contact forces between ballast particles and those between the ballast and the sleepers. Each line is orientated along the direction of the contact force it represents and its thickness is proportional to the force magnitude. It can be observed that large contact forces are generated near the sleeper end and diffused to the shoulder ballast to provide resistance to the sleeper movement in all the four cases. For the ballasted track without the polyurethane, the maximum contact force between the ballast and the sleeper end is 650 N. When the polyurethane is applied to reinforce the ballast near the sleeper ends, near the sleeper centre and at both areas, respectively, the maximum contact force increases to 1235.7 N, 976.4 N and 1561.9 N. The maximum contact force increases by 90.1%, 50.2% and 1.4 times, respectively.

According to the DEM results, for the ballasted track without the polyurethane, the maximum particle displacement is 3.13 mm when the lateral sleeper displacement *d* reaches 3 mm. When the polyurethane is applied to reinforce the ballast near the sleeper ends, near the sleeper centre and at both regions, the maximum particle displacement decreases to 2.91 mm, 2.98 mm and 2.84 mm, respectively. The maximum particle displacement decreases by 7%, 4.8% and 9.3%, respectively. Apparently, the maximum particle displacement of the ballast was restrained to a certain degree due the bonding effect of the polyurethane to the ballast particles.

From the contact force chains and particle displacement results, it can be understood that the polyurethane successfully restrains the ballast particle movement and improves the load-bearing capacity of the granular ballast at the particle scale. This is because the polyurethane provides strong bonding effect to the ballast particles so that effectively restrains the particle movement induced by the squeezing and friction effect of the sleeper. With the large-area and effective bonding of the polyurethane, the granular ballast particles are integrated to form a more stable load-bearing structure. Hence, the polyurethane-reinforced ballast can provide larger resistance force to the sleeper by restraining the particle movement inside it and increasing the contact force network intensity.

5 Conclusions

This paper has proposed three new bonding schemes to reinforce the ballast with polyurethane more efficiently by merely bonding the ballast near the sleeper ends or centre, or in both areas. Whereas the shoulder ballast height is cancelled and the bonding area is small, the lateral resistance of the polyurethane-reinforced ballast with the application of the new bonding schemes were investigated in the paper.

A series of single sleeper pull-out tests were carried out to study the lateral resistance force-displacement responses of the reinforced ballast. The test results indicated that if the ballast was reinforced with polyurethane based on the proposed bonding schemes, the ballast resistance was larger than that of the ordinary ballast without any reinforcement by at least 31%. These results demonstrate that all the three new bonding schemes can ensure adequate ballast lateral resistance to keep track stability.

Discrete element models were also established to simulate the SSPTs using clumps with realistic particle shapes. Parallel bonds were created in the models to simulate the bonding effect of the polyurethane to the ballast particles. The simulation results of the DEM models showed good agreement with the laboratory test results. According to the DEM results, the particle displacement and the contact force chains were analysed to investigate the micro-mechanical behaviours of the reinforced ballast. It was found that the bonding effect of the polyurethane at the particle scale can effectively restrain the movement of ballast particles and thereby successfully integrate the granular ballast to form a more stable load-bearing structure, which provides larger ballast resistance force to the sleeper than the ordinary granular ballast.

After the evaluation of ballast resistance in this study, the proposed bonding schemes have the advantages of mitigating the ballast flight, saving the dosage of the polyurethane, having negligible influence to the tamping operation and providing adequate ballast resistance simultaneously. These bonding schemes can be chosen by engineers to mitigate the ballast flight risk in the high-speed railways or to increase the ballast resistance effectively.

Acknowledgements

This work is supported by the Natural Science Foundation of China (NSFC) project under grant No. 51578051 and the Guangdong University of Technology Youth Fund under grant 18QNZD002.

References

[1] Esveld, C. (2001). Modern railway track, second edition. MRT-productions, The Netherlands.

[2] Esmaeili, M., Khodaverdian, A., Neyestanaki, H. K., & Nazari, S. (2016). Investigating the effect of nailed sleepers, on increasing the lateral resistance of ballasted track. Computers & Geotechnics, 71, 1-11.

[3] Esmaeili, M., Zakeri, J. A., & Babaei, M. (2017). Laboratory and field investigation of the effect of geogrid-reinforced ballast on railway track lateral resistance. Geotextiles & Geomembranes, 45(2), 23-33.

[4] Kasraei, A., Zakeri, J. A., Esmaeili, M., & Bakhtiary, A. (2016). A numerical investigation on the lateral resistance of frictional sleepers in ballasted railway tracks. Proceedings of the Institution of Mechanical Engineers, Part F: Journal of Rail & Rapid Transit, 10(6), 1-10.

[5] Koike, Y., Nakamura, T., Hayano, K., & Momoya, Y. (2014). Numerical method for evaluating the lateral resistance of sleepers in ballasted tracks. Soils & Foundations, 54(3), 502-514.

[6] Tutumluer, E., Huang, H., Hashash, Y., and Ghaboussi, J. (2006). Aggregate shape effects on ballast tamping and railroad track lateral stability. Proc., Annual Conf. of the American Railway Engineering and Maintenance-of-Way Association, American Railway Engineering and Maintenance-of-Way Association, Lanham, MD.

[7] Quinn, A. D., Hayward, M., Baker, C. J., Schmid, F., Priest, J. A., & Powrie, W. (2010). A full-scale experimental and modelling study of ballast flight under high-speed trains. Proceedings of the Institution of Mechanical Engineers, Part F: Journal of Rail & Rapid Transit, 224(2), 61-74.

[8] Premoli, A., Rocchi, D., Schito, P., Somaschini, C., & Tomasini, G. (2015). Ballast flight under high-speed trains: wind tunnel full-scale experimental tests. Journal of Wind Engineering & Industrial Aerodynamics, 145, 351-361.

[9] Jönsson, M., Ehrenfried, K., Loose, S., & Wagner, C. (2014). Particle image velocimetry of the underfloor flow of generic high-speed train models in a water towing tank. Proceedings of the Institution of Mechanical Engineers, Part F: Journal of Rail & Rapid Transit, 228(2), 194-209.

[10] Goo, J. S., Kim, J. S., & Shin, K. B. (2015). Evaluation of structural integrity after ballast-flying impact damage of a grip lightweight bogie frame for railway vehicles. Journal of Mechanical Science & Technology, 29(6), 2349-2356.

[11] Le Pen, L., & Powrie, W. (2011). Contribution of base, crib, and shoulder ballast to the lateral sliding resistance of railway track: a geotechnical perspective. Proceedings of the Institution of Mechanical Engineers, Part F: Journal of Rail & Rapid Transit, 225(2), 113-128.

[12] Lee S. H., Lee, S. J., Park, J. G., & Choi, Y. T. (2017). An experimental study on the characteristics of polyurethane-mixed coarse aggregates by large-scale triaxial test. Construction & Building Materials, 145, 117-125.

[13] Woodward, P. K., Kacimi, A. E., Laghrouche, O., Medero, G., & Banimahd, M. (2012). Application of polyurethane geocomposites to help maintain track geometry for high-speed ballasted railway tracks. Journal of Zhejiang University-Science A (Applied Physics & Engineering), 13(11), 836-849.

[14] Woodward, P. K., Kennedy, J., Medero, G. M., & Banimahd, M. (2012). Maintaining absolute clearances in ballasted railway tracks using in situ three-dimensional polyurethane geocomposites. Proceedings of the Institution of Mechanical Engineers, Part F: Journal of Rail & Rapid Transit, 226(226), 257-271.

[15] Woodward, P. K., Kennedy, J., Laghrouche, O., Connolly, D. P., & Medero, G. (2014). Study of railway track stiffness modification by polyurethane reinforcement of the ballast. Transportation Geotechnics, 1(4), 214-224.

[16] Kennedy, J., Woodward, P. K., Medero, G., & Banimahd, M. (2013). Reducing railway track settlement using three-dimensional polyurethane polymer reinforcement of the ballast. Construction & Building Materials, 44(3), 615-625.

[17] Woodward, P. K., Kennedy, J., Medero, G. M., & Banimahd, M. (2012). Application of in situ polyurethane geocomposite beams to improve the passive shoulder resistance of railway track. Proceedings of the

Institution of Mechanical Engineers, Part F: Journal of Rail & Rapid Transit, 226(3), 294-304.

[18] Kruglikov, A. A. Yavna, V. A. & Ermolov, Y. M. (2017). Strengthening of the railway ballast section shoulder with two-component polymeric binders. Transportation Geotechnics, 11: 133-143.

[19] Thomas, S., Woodward, P., & Laghrouche, O. (2015). Influence of stiffening ballasted track bed overlying a masonry arch bridge using a polyurethane polymer material. Construction & Building Materials, 92, 111-117.

[20] National Railway Administration of P.R. China. (2014). Code for design of high speed railways. China Railway Press, Beijing. (in Chinese)

[21] Cundall, P. A., & Strack, O. D. L. (1979). A discrete numerical model for granular assemblies. Geothechnique, 29(30), 331-336.

[22] Chen, C., Mcdowell, G. R., and Thom, N. H. (2012). Discrete element modelling of cyclic loads of geogrid-reinforced ballast under confined and unconfined conditions. Geotextiles and Geomembranes, 35(35):76-86.

[23] Indraratna, B., Ngo, N. T., Rujikiatkamjorn, C., and Vinod, J. S. (2012). Behaviour of fresh and fouled railway ballast subjected to direct shear testing: discrete element simulation. International Journal of Geomechanics, 14(1):34-44.

[24] Tutumluer, E., Qian, Y., Hashash, Y. M. A., Ghaboussi, J., and Davis, D. D. (2013). Discrete element modelling of ballasted track deformation behaviour. International Journal of Rail Transportation, 1(1-2):57-73.

[25] Zhang, X., Zhao, C., & Zhai, W. (2017). Dynamic behavior analysis of high-speed railway ballast under moving vehicle loads using discrete element method. International Journal of Geomechanics, 17(7): 04016157.

[26] Zhang X., Zhao C. & Zhai W. (2019). Importance of load frequency in applying cyclic loads to investigate ballast deformation under high-speed train loads. Soil Dynamics and Earthquake Engineering, 120:28-38.

[27] Ling, X., Xiao, H., & Cui, X. (2018). Analysis of mechanical properties of polyurethane-mixed ballast based

on energy method. Construction & Building Materials, 182, 10-19.

[28] Itasca Consulting Group. (2008). Particle flow code in three dimensions (PFC3D), Minneapolis.

[29] Anochie-Boateng, J. K., Komba, J. J., & Mvelase, G. M. (2013). Three-dimensional laser scanning technique to quantify aggregate and ballast shape properties. Construction & Building Materials, 43(43), 389-398.

Table list:

Table 1 Mechanical properties of the polyurethane used in the test

Parameter	Value
Density (g/cm^3)	1.13
Tensile strength (MPa)	14.2
Elongation at break (%)	20
Tearing strength (N/mm)	60
Shore hardness	46

Table 2 Summary of the tests carried out in the laboratory

Test name	Shoulder height (mm)	Bonding area	Bonding depth from the top surface (mm)
Ns	150	None	0
Nf	0	None	0
E2	0	At sleeper ends	200
E3	0	At sleeper ends	300
C2	0	near sleeper center	200
C3	0	near sleeper center	300
B2	0	both areas	200
B3	0	both areas	300

Table 3 Lateral resistance forces of ballast at *d*= 2mm in various tests and their differences

Test	Lateral resistance force (kN)	Difference from Ns	Difference from Nf
Ns	10.0	-	42%
Nf	7.05	-30%	-
E2	14.09	41%	100%
E3	16.07	60%	128%
C2	13.09	31%	86%
C3	14.09	41%	100%
B2	17.08	70%	142%
B3	20.02	100%	184%

Table 4 The micro-mechanical parameters in the DEM simulations

Parameters	Value	Parameters	Mean value	Standard error
Damping coefficient	0.5	Parallel bonds		
Ballast particles		Normal stiffness (N/m^2)	1.5×10^7	1.0×10^6
Clump density (kg/m^3)	2700	Shear stiffness (N/m^2)	1.5×10^7	1.0×10^6
Normal stiffness (N/m)	1×10^8	Tensile strength (Pa)	1.42×10^7	1.0×10^6
Shear stiffness (N/m)	1×10^8	Cohesive strength (Pa)	1.42×10^7	1.0×10^6
Friction coefficient	0.5	Friction angle (°)	45	0
Ballast-sleeper contacts				
Normal stiffness (N/m)	5×10^9			
Shear stiffness (N/m)	5×10^9			
Friction coefficient	0.5			

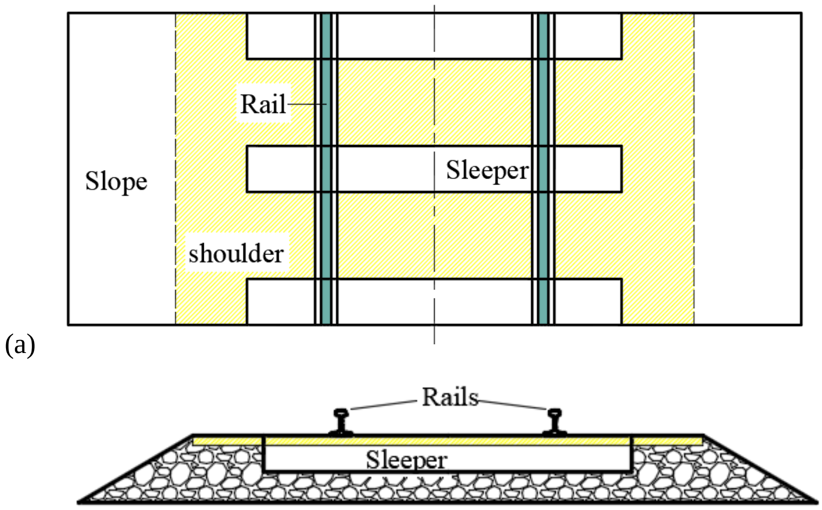

Fig. 1 Sketch of the target region (in yellow) in the conventional bonding scheme for reinforcing the ballast with polyurethane: (a) plane view and (b) end view

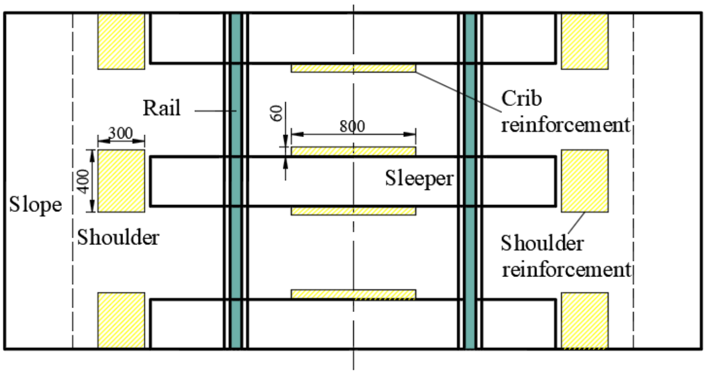

Fig. 2 Sketch of the target regions (in yellow) in the new bonding schemes for reinforcing the ballast with polyurethane (unit: mm)

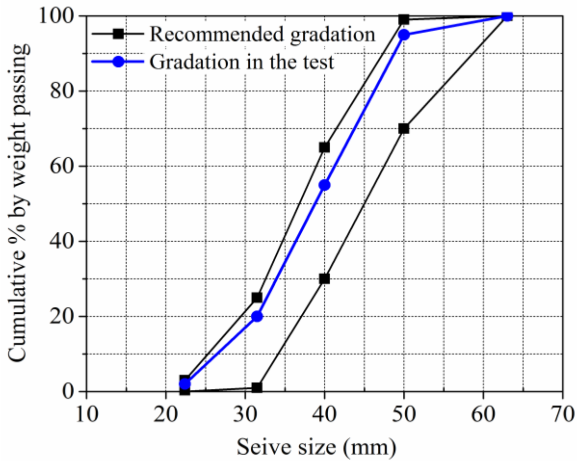

Fig. 3 Particle size gradation of ballast in the tests

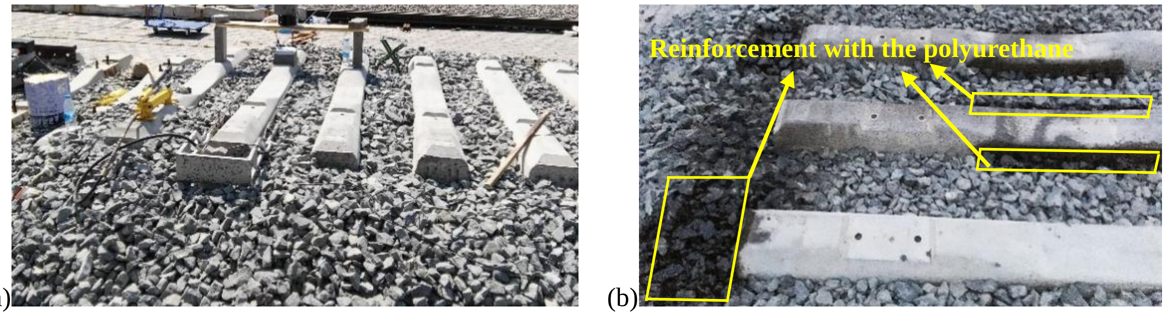

(a) (b)

Fig. 4 Photographs of the ballasted track with and without the reinforcement of the polyurethane: (a) without reinforcement, (b) reinforced at both regions

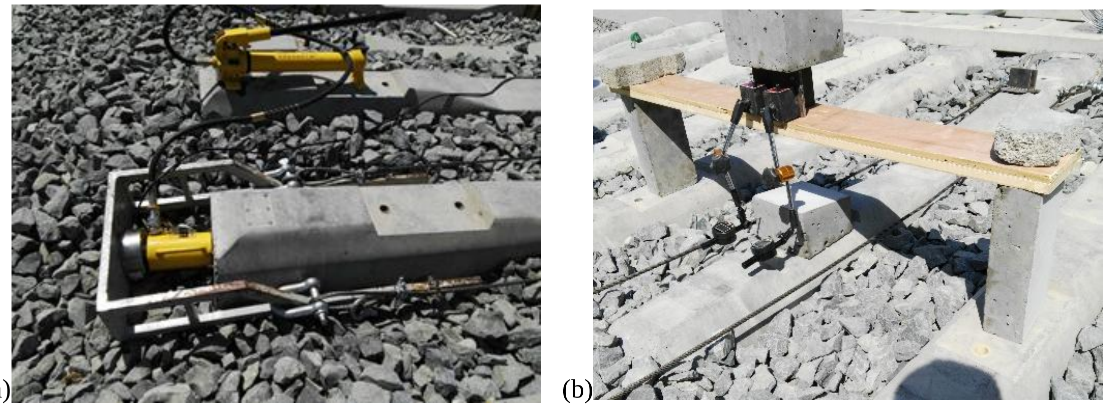

(a) (b)

Fig. 5 Apparatus for measuring (a) the lateral resistance force of the ballast and (b) the lateral displacement of the sleeper

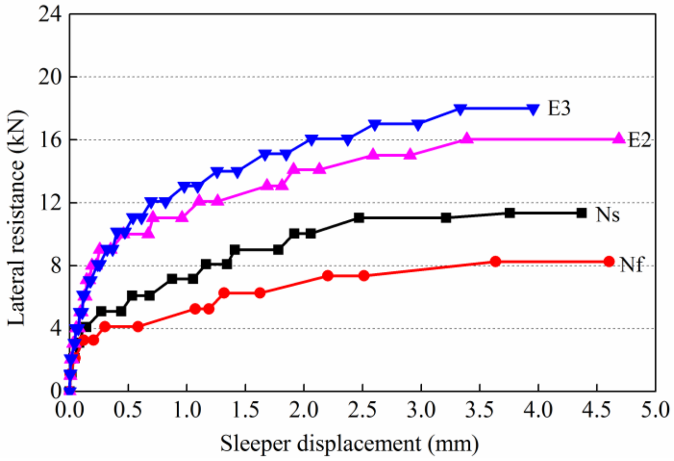

a)

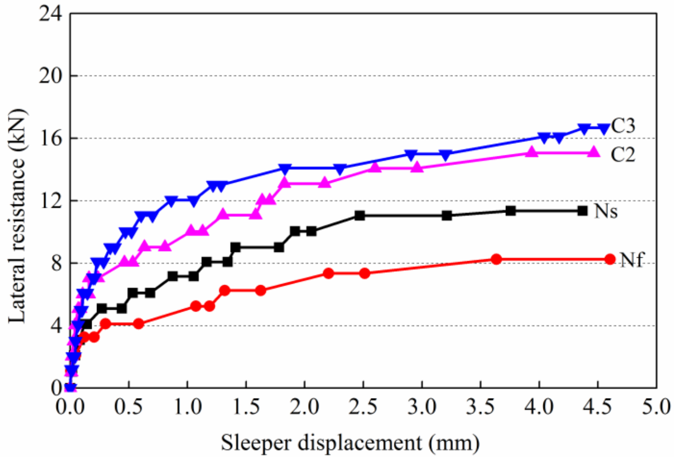

b)

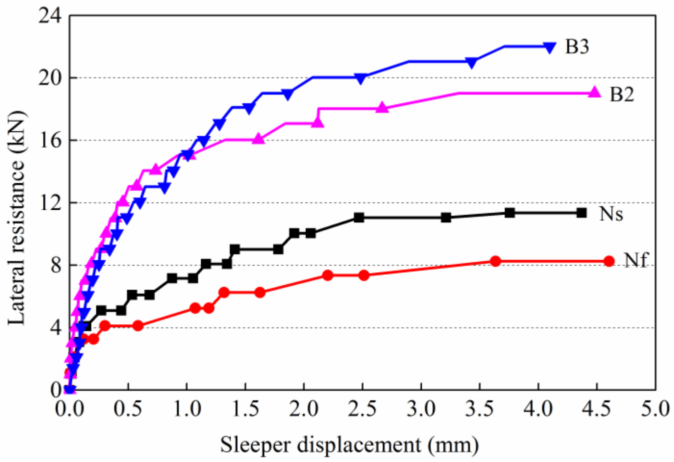

c)

Fig. 6 Test results of the lateral resistance force-displacement responses of the reinforced ballast based on various bonding schemes: (a) reinforced near the sleeper ends, (b) reinforced near the sleeper centre and (c) reinforced at both regions

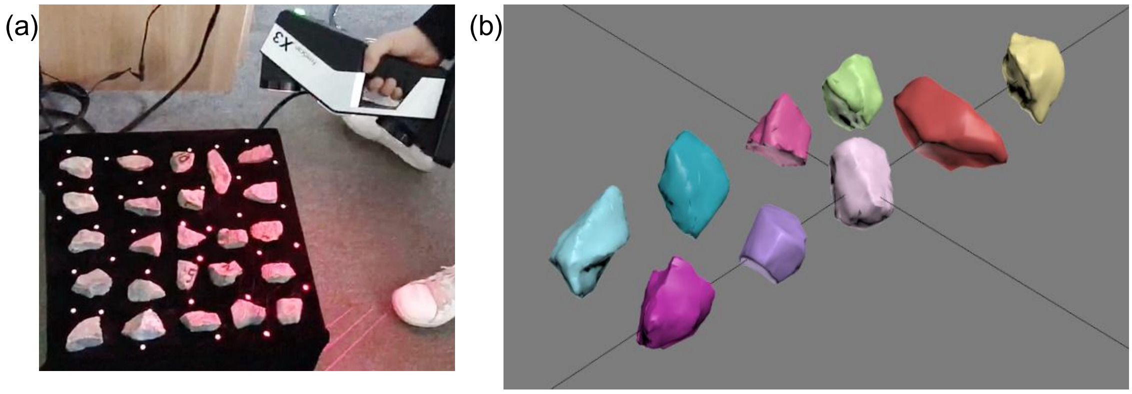

Fig. 7 3D laser scanning of ballast particles: (a) photograph of scanning and (b) the scanned images

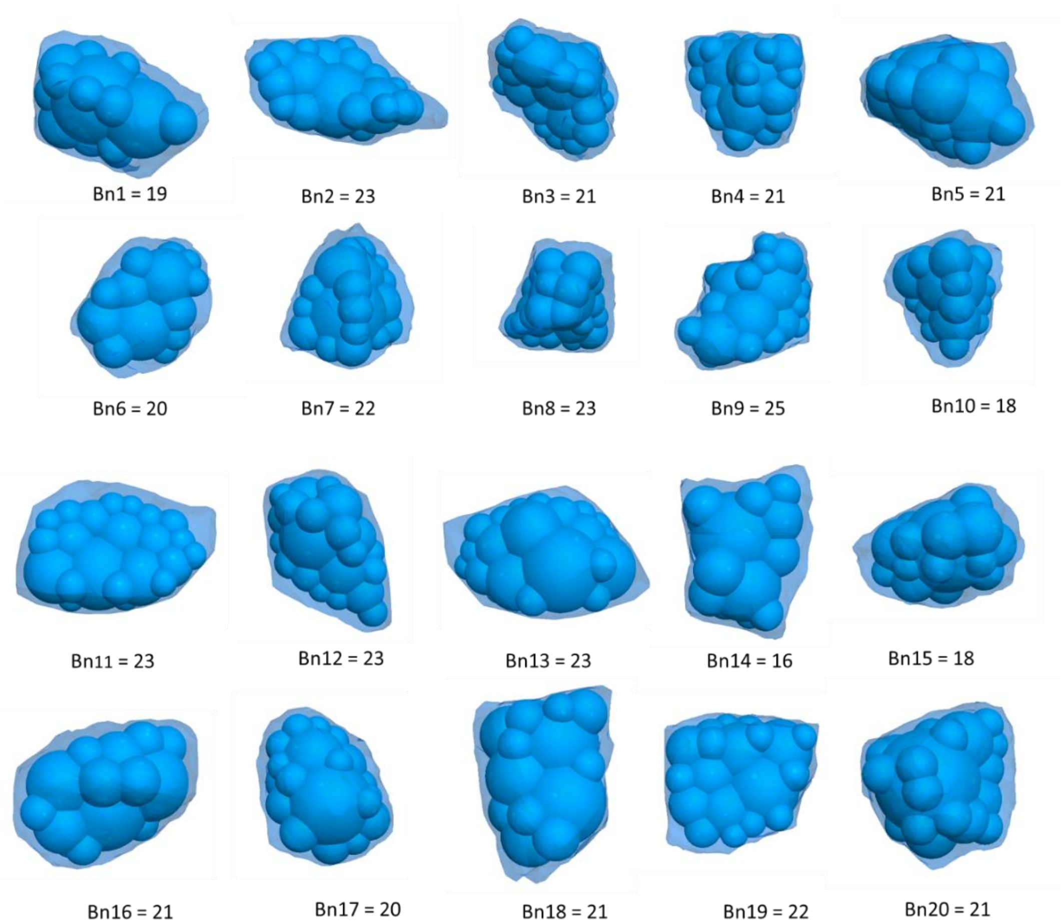

Fig. 8 Ballast particle shapes and clumps generated in PFC

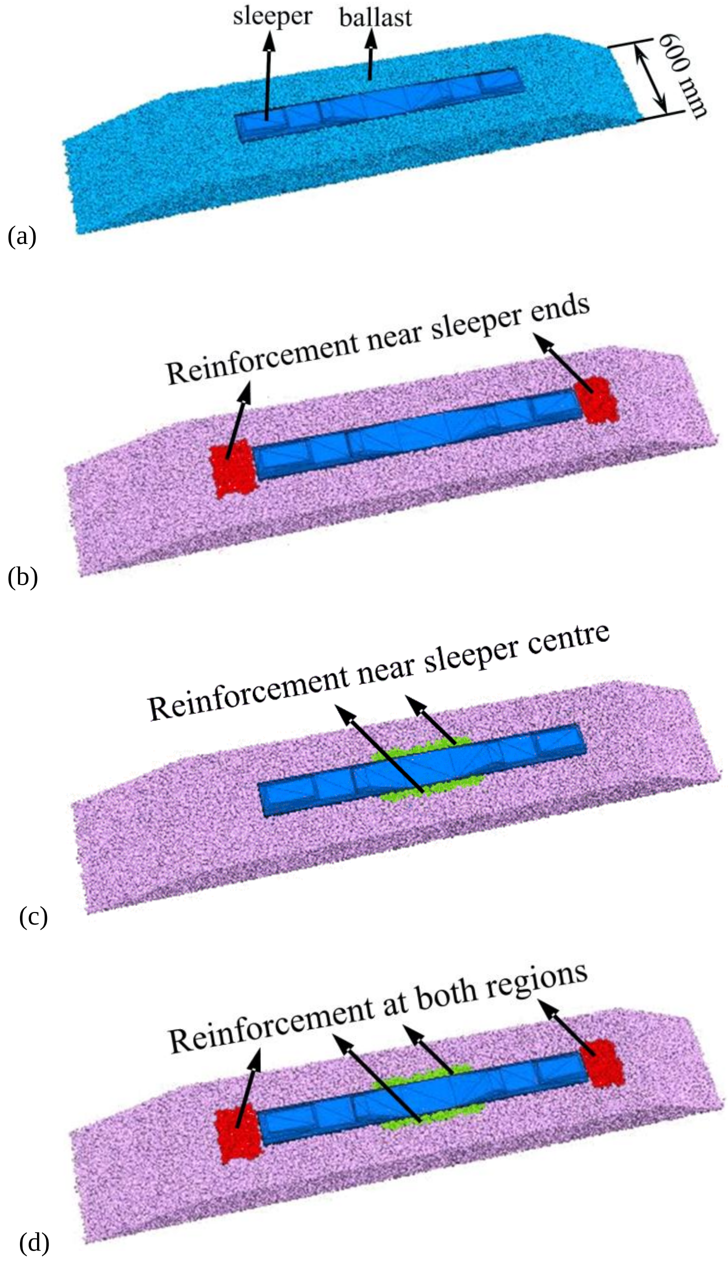

Fig. 9 The DEM models of the sleeper-ballast structure with and without the reinforcement of polyurethane: (a)without reinforcement, (b)reinforced near the sleeper ends, (c)reinforced near the sleeper centre and (d)reinforced at both regions

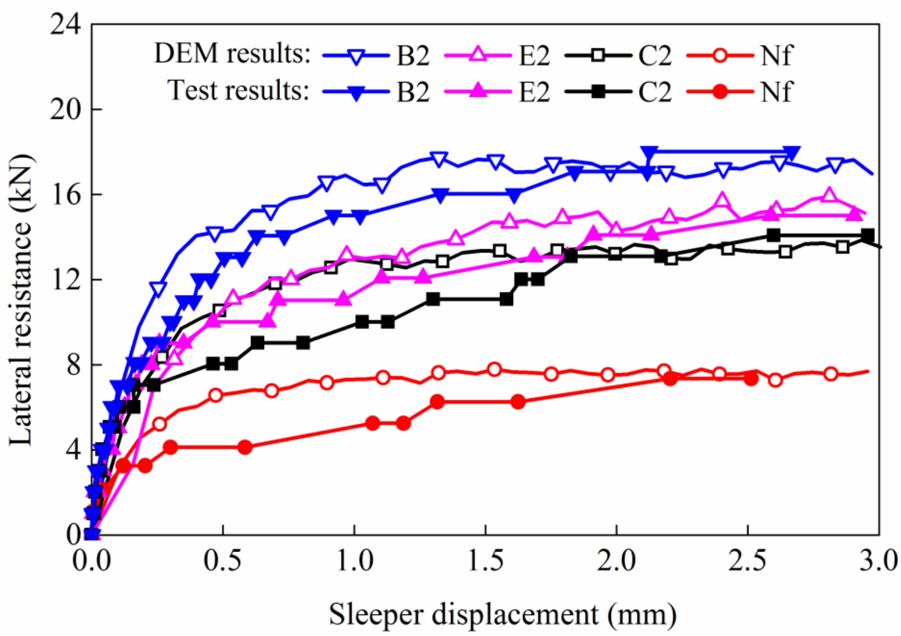

Fig.10 The resistance force-displacement responses of the reinforced ballast: a comparison between the DEM and test results

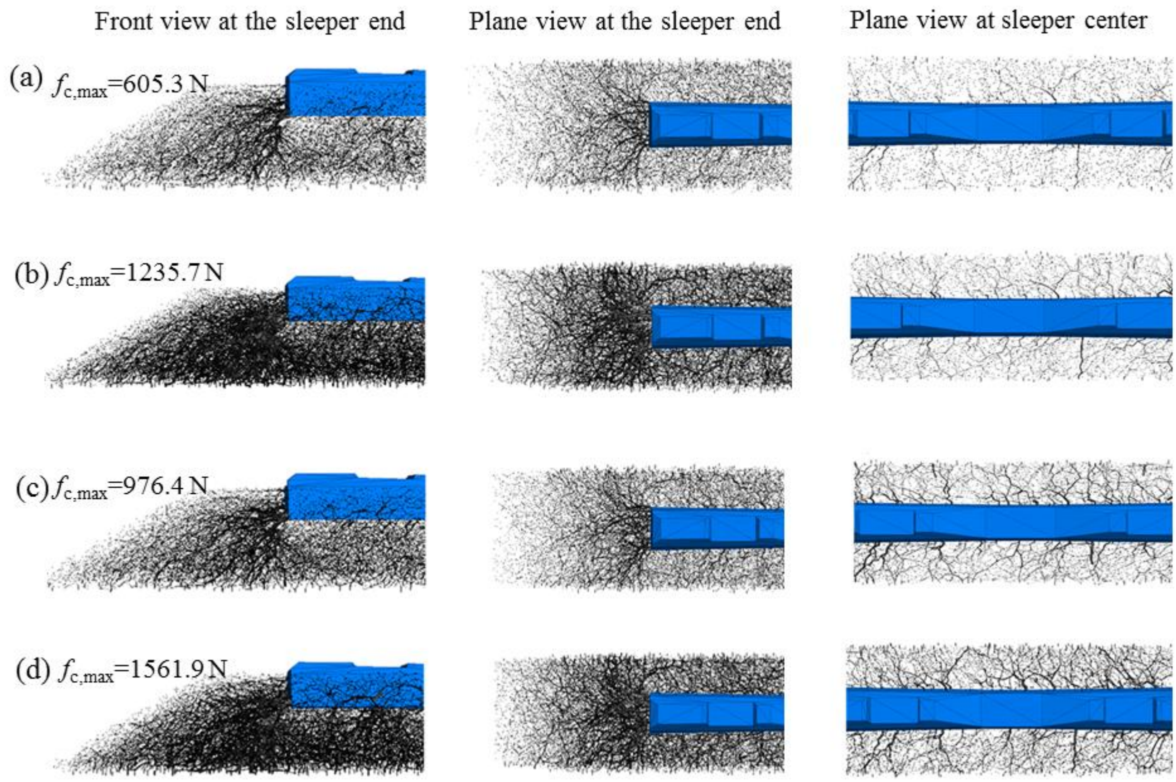

Fig.11 Contact force chains distributions in the ballast at d=3mm: (a) unreinforced ballast, (b) reinforced near the sleeper ends, (c) reinforced near the sleeper centre and (d) reinforced at both regions